Characteristics of Whipple shield performance in the shatter regime

S. Ryan[*,1], M. Bjorkman[2], E. L. Christiansen[3]

[1]*USRA Lunar and Planetary Institute, 3600 Bay Area Blvd, Houston, TX, 77058, USA*
[2]*Jacobs Engineering, 2224 Bay Area Blvd, Houston, TX, 77058, USA*
NASA Johnson Space Center, 2101 NASA Pkwy, Houston, TX, 77058, USA

Abstract

Ballistic limit equations define the failure of metallic Whipple shields in three parts: low velocity, shatter, and hypervelocity. Failure limits in the shatter regime are based on a linear interpolation between the onset of projectile fragmentation, and impulsive rupture of the shield rear wall. A series of hypervelocity impact tests have been performed on aluminum alloy Whipple shields to investigate failure mechanisms and performance limits in the shatter regime. Test results demonstrated a more rapid increase in performance than predicted by the latest iteration of the JSC Whipple shield BLE following the onset of projectile fragmentation. This increase in performance was found to level out between 4.0-5.0 km/s, with a subsequent decrease in performance for velocities up to 6.0 km/s. For a detached spall failure criterion, the failure limit was found to continually decrease up to a velocity of 7.0 km/s, substantially varying from the BLE, while for perforation-based failure an increase in performance was observed. An existing phenomenological ballistic limit curve was found to provide a more accurate reproduction of shield behavior that the BLE, however a number of underlying assumptions such as the occurrence of complete projectile fragmentation and the effect on performance of incipient projectile melt were found to be inaccurate. A cratering relationship based on the largest residual fragment size has been derived for application at velocities between 3.0-4.0 km/s, and was shown to accurately reproduce the trends of the experimental data. Further investigation is required to allow a full analytical description of shatter regime

*Corresponding author. Tel.: +1 281 413-2983; fax: +1 281 483-3908.
E-mail address: shannon.j.ryan@nasa.gov

performance for metallic Whipple shields.

Nomenclature

d	Diameter (cm)	b	Bumper
S	Shield spacing (cm)	c	Critical
t	Thickness (cm)	f	Fragment
V	Velocity (km/s)	p	Projectile
θ	Impact angle (deg)	w	Rear wall
ρ	Density (g/cm^3)	LV	Low velocity
σ	Yield strength (ksi)	HV	Hypervelocity

1. Introduction

In 1947 Fred Whipple suggested that a thin "bumper", when placed in front of a space vehicles pressure hull, would substantially increase the vehicle's level of protection against impacting meteors. From Apollo through Space Station, the Whipple shield concept has provided the baseline for shielding against the impact of micrometeoroids and orbital debris (MMOD). Over the range of impact velocities relevant for Earth-orbiting spacecraft, the performance of a Whipple shield is characterized in three parts: low velocity, shatter, and hypervelocity. In the low velocity regime, the projectile remains intact during penetration of the shield bumper plate, leading to impact of an intact (albeit possibly deformed and eroded) projectile upon the shield rear wall. Transition to the shatter regime occurs once the impact shock amplitudes are sufficient to induce fragmentation of the projectile. Within the shatter regime, further increases in projectile velocity result in increased projectile fragmentation, transitioning from a small number of solid fragments to a multitude of small, finely dispersed mixed phase debris cloud (solid and molten fragments). Transition to the hypervelocity regime is defined by the point at which the rear wall failure mechanism changes from cratering-based to impulsive, similar to that induced by a

gaseous blast wave. Increased impact speeds within the hypervelocity regime are expected to increase the debris cloud kinetic energy, resulting in a decrease in shielding performance.

Ballistic limit equations (BLEs) are used to design and evaluate the performance of shields for MMOD protection. For a metallic Whipple shield, the new non optimum equation (NNO) [1], or variations thereof (e.g. [2]) are commonly used. These equations are based on cratering relationships in the low velocity regime, momentum conservation in the hypervelocity regime, and a linear interpolation between the two in the shatter regime. With a debris environment increasingly dominated by manmade debris, vehicles operating in low earth orbit (LEO) are subject to slower median encounter velocities. As such, the performance of shielding at velocities in the shatter regime is increasingly important to mission risk predictions. In this paper, the results of an experimental impact study to characterize failure limits of an aluminum alloy Whipple shield in the shatter regime are presented.

2. Predicting the failure limit of metallic Whipple shields

The most recent iteration of the Whipple shield ballistic limit equation is based on the NNO approach and incorporates a selection of modifications proposed by Reimerdes et al. [2].

In the low velocity regime, i.e. $V < V_{LV}$:

$$d_c = \left[\frac{t_w \left(\sigma/40\right)^{0.5} + t_b}{0.6\left(\cos\theta\right)^{5/3} \rho_p^{0.5} V^{2/3}} \right]^{18/19} \tag{1}$$

where,

$$V_{LV} = \begin{cases} 1.436\left(t_b/d_p\right)^{-1/3} & , t_b/d_p < 0.16 \\ 2.60 & , t_b/d_p \geq 0.16 \end{cases} \tag{2}$$

In the hypervelocity regime, i.e. $V \geq 7$:

$$d_c = 3.918 \, F_2^* \frac{t_w^{2/3} S^{1/3} \left(\sigma/70\right)^{1/3}}{\rho_p^{1/3} \rho_b^{1/9} \left(V \cos \theta\right)^{2/3}}$$

(3)

where F_2^* is a de-rating factor which accounts for the detrimental effect on projectile fragmentation (and hence, shielding performance) for insufficiently thick bumper plates, i.e.:

$$F_2^* = \begin{cases} 1 & for \quad \left(t_b/d_p\right) \geq \left(t_b/d_p\right)_{crit} \\ r_{S/D} - 2\frac{\left(t_b/d_p\right)}{\left(t_b/d_p\right)_{crit}}\left(r_{S/D} - 1\right) + \left(\frac{\left(t_b/d_p\right)}{\left(t_b/d_p\right)_{crit}}\right)^2 \left(r_{S/D} - 1\right) & for \quad \left(t_b/d_p\right) < \left(t_b/d_p\right)_{crit} \end{cases}$$

(4)

where,

$$\left(t_b/d_p\right)_{crit} = \begin{cases} 0.2\left(\rho_p/\rho_b\right) & for \quad S/d_p \geq 30 \\ 0.25\left(\rho_p/\rho_b\right) & for \quad S/d_p < 30 \end{cases}$$

(5)

and $r_{S/D}$ is ratio between the required rear wall thickness when the bumper thickness is zero, and when it is equal to the limit $(t_b/d_p)_{crit}$, i.e.:

$$r_{S/D} = \frac{t_w\left(t_b = 0\right)}{t_w\left(t_b/d_p = \left(t_b/d_p\right)_{crit}\right)} = \frac{\left(0.6 \cdot d_p^{19/18}\left(\cos\theta\right)^{5/3}\rho_p^{0.5}V_{HV}^{2/3} - t_b\right)\big/\left(\sigma/40\right)^{0.5}}{\left(d_p\big/3.918 \cdot \rho_p^{-1/3}\rho_b^{-1/9}\left(V_{HV}\cos\theta\right)^{-2/3}S^{1/3}\left(\sigma/70\right)^{1/3}\right)^{3/2}}$$

(6)

Linear interpolation is used in the shatter regime, i.e. $V_{LV} < V < V_{HV}$:

$$d_c = d_c\left(V_{LV}\right) + \frac{\left(d_c\left(V_{HV}\right) - d_c\left(V_{LV}\right)\right)}{V_{HV} - V_{LV}} \times \left(V_n - V_{LV}\right)$$

(7)

Although providing a reasonable and conservative simplification of shield performance for risk assessment, the linear interpolation in the shatter regime may not accurately reproduce the actual behavior observed for this shield type. In 1970, Swift et al. [6] reported on a series of hypervelocity impact experiments that were performed on aluminum shields with constant spacing and bumper

thickness, while the shield rear wall thickness was varied in order to determine the failure threshold. In this series of experiments, failure was defined as the limit between puncture and no puncture, evaluated via dye penetrant and gas leak criterion. To effectively describe the types of damages observed in target photographs, and in an effort to better characterize the impact performance of a dual-wall structure, Hopkins et al. [4] defined a phenomenological ballistic limit curve (BLC), shown in Fig. 1. In region I, the typical damage observed was a single crater – indicating an intact projectile. In region II, typical damage graduated from a few fairly large craters to a multitude of small craters as a result of the onset and escalation of projectile fragmentation. In region III, the appearance of damage remained rather constant, with each individual crater increasing in size and depth. In region IV, solid fragment craters similar in appearance to those in region II/III were increasingly interspersed by soft contour craters made by molten fragments. Throughout region V, soft contour craters caused by molten material were the dominant damage observable. Region VI damage was characterized by a mixture of molten and vapor damage, where the failure transitions from penetration and perforation to rupture and tearing at the upper velocity limits. Damage in region VII was similar to that of pressing by high-pressure gas.
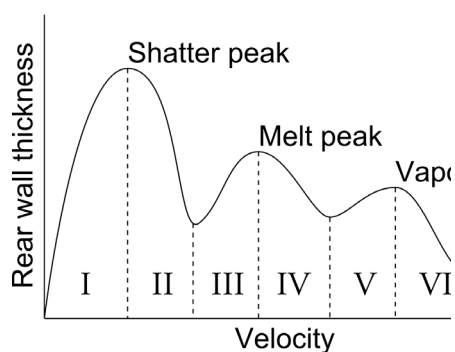

Fig. 1. Phenomenological ballistic limit curve for an Al-alloy Whipple shield (reproduced from [4])

The phenomenological BLC is reproduced Fig. 2 together with test data from [6], and is shown to provide a significantly better reproduction of the experimental trends than the NNO BLE [1].
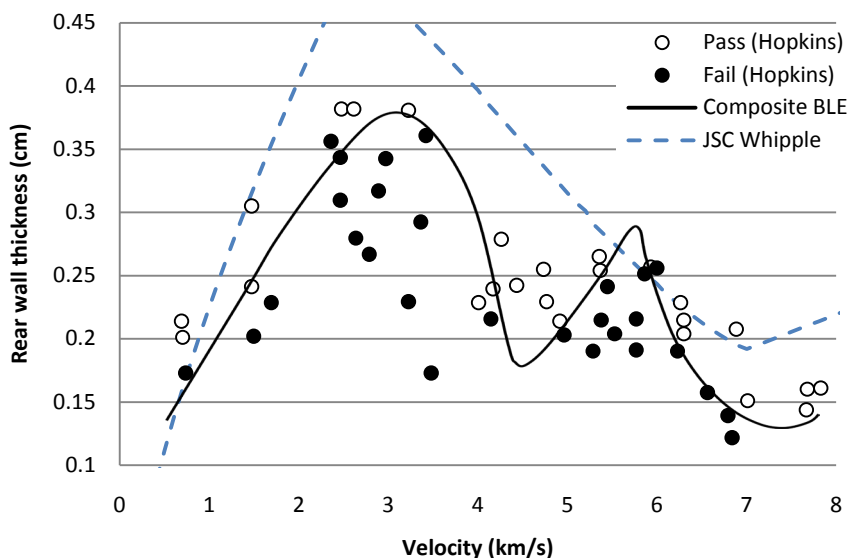
Fig. 2. Comparison of the phenomenological and NNO ballistic limit curves with test data (reproduced from [5]). Test configuration: t_b = 0.079 cm (Al6061-T6), S = 5.08 cm, θ = 0°, d_p = 0.3175 cm.

The transition velocities for the phenomenological ballistic limit curve can be inferred from [4] as:

- Region I: V < 3.1 km/s

- Region II: 3.1 < V < 4.4 km/s

- Region III: 4.4 < V < 5.6 km/s

- Region IV: 5.6 < V < 7.0 km/s

- Region V: V > 7 km/s

The upper limit of region I refers to the onset of projectile fragmentation, which is commonly defined for aluminum on aluminum impact at 3.0 km/s (e.g. [1]). Velocities for incipient and complete melt are assumed to be based on 1-D entropy trapping calculations (e.g. [4]). For aluminum-on-aluminum impacts, the upper limits for region III and IV are calculated as 5.62 and 7.04 km/s respectively (A = 0.1704 Mb; γ = 4.3; Γ = 2.0).

Concurrent to the research of Swift and Hopkins, Nysmith [3] investigated failure modes of double-sheet Whipple shield structures and defined failure limits, or ballistic limit curves, based on the physical processes by which the shield rear wall failed. He found that, for particular shield configurations, the velocity of a constant mass projectile required to perforate the shield rear wall was double-valued, i.e. there exists a range between two failure velocities in which failures do not occur (see h_c/d in Fig. 3). This occurred as a result of the changing state of material in the debris cloud following impact and perforation of the bumper plate, and the distance separating the bumper from the shield rear wall.
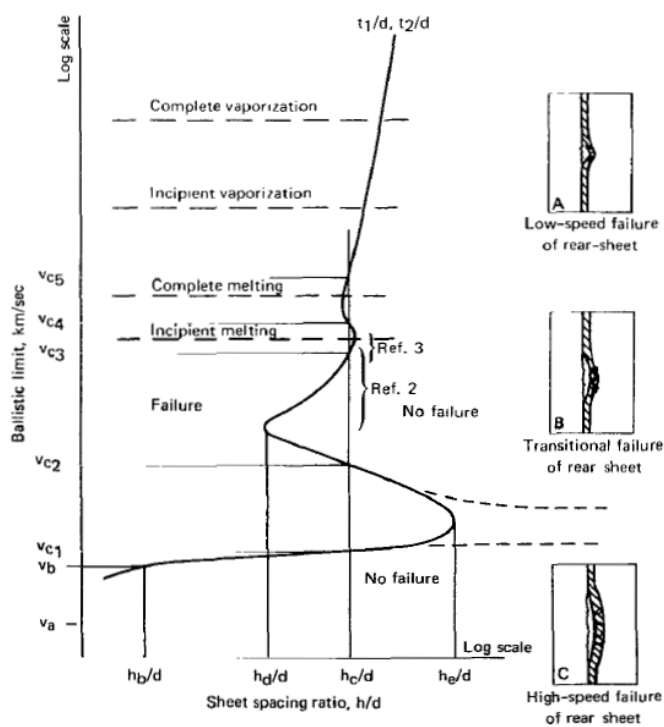

Fig. 3. Hypothetical performance curve for double sheet structures (from [3])

A series of hypervelocity impact tests have recently been performed at NASA JSC's White Sand's Test Facility to reproduce the experimental findings of Swift et al. The purpose of these experiments is

to investigate the claim of Swift, Hopkins, Nysmith etc. that the ballistic performance of Whipple shield structures in the shatter regime substantially deviates from the linear approximation of current BLEs used in mission risk assessment. In this paper, the results of the test program, along with an analysis of shield failure mechanism and the corresponding role of material phase in the debris cloud are discussed. As the metallic Whipple shield represents one of the most simple and widely applied shielding configurations, a better understanding of failure processes and mechanisms will aid in the design and evaluation of new shield types.

3. Impact Testing

A total of 82 successful impact tests were performed on aluminum alloy Whipple shields nominally identical to those tested by Swift et al. in [6]. The thickness of the Al6061-T6 bumper (t_b = 0.079 cm), shield spacing (S = 5.08 cm) and projectile diameter (d_p = 0.3175 cm) were constant, while the Al6061-T6 rear wall thickness (t_w) was modified in order to determine the ballistic limits of the shield. Tests were performed at varying impact angles (0°/45°/60°) and over a range of velocities from 2.27-7.20 km/s. In all the tests, failure was defined as the ejection of any material into the simulated pressure hull (i.e. detached spall, SP), however distinction was made between spalled targets and those clearly perforated (P). It should be noted that the failure criteria is different to that used in the original investigation, which assessed failure through use of dye penetrant or gas leak (i.e. perforation). A schematic of the test configuration is shown in Fig. 4.

A summary of the test conditions and results is given in Table 1. Of the 82 tests there were 23 perforated targets, 17 spalled targets, and 42 pass results. It is interesting to note that only 1 of the 17 detached spall results were achieved in oblique incidence tests.
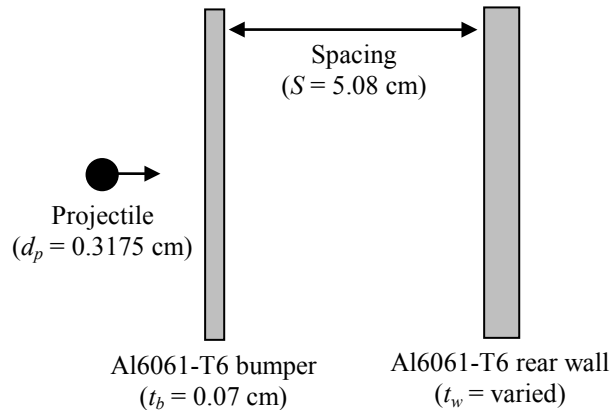
Fig. 4. Schematic of the Whipple shield test setup.

In Fig. 5 and Fig. 6 the test results at 0° and 45° are plotted against the JSC Whipple shield BLE (Eq. (1)-(7)). There are three key findings in the figures, namely:

1. Following the onset of projectile fragmentation, shield performance improves more rapidly in the shatter regime than predicted by the BLE,

2. In the upper ranges of the shatter regime, shield performance is found to decrease with increasing impact velocity,

3. Detached spallation limits in normal incidence tests at velocities between 5.8-6.9 km/s are significantly under predicted by the BLE.

Fig. 7 and Fig. 8 show a series of rear wall damage photographs for normal incidence tests with impact velocities between 2.6-6.9 km/s. A clear progression from solid projectile impact (HD9920118), to fragmentation initiation (HD9902117), through increasing degrees of fragmentation (HD9920060-HD9920057) and the onset of melting (HD9920159-HD9920116) can be observed on the front side of the targets, which corresponds well with the descriptions from [4]. The rear side view shows that the targets all fractured internally (incipient spall) without any detachment of material.

Table 1. Overview of Whipple shield test conditions and results

| Test no.	θ (deg)	V (km/s)	t_w (cm)	Result	Test no.	θ (deg)	V (km/s)	t_w (cm)	Result
HD9920118	0	2.6	0.4572	NP	HD0020010	45	6.50	0.4064	NP
HD9920117	0	3	0.4572	NP	HD0020122	45	6.53	0.254	NP
HD9920060	0	4.7	0.254	NP	HD0020047	45	6.60	0.3175	NP
HD9920057	0	5.5	0.3175	NP	HD0020053	45	7.20	0.3175	NP
HD9920159	0	6	0.4064	NP	HD9920272	45	3.10	0.3175	P
HD9920151	0	6.6	0.4064	NP	HD0020011	45	4.50	0.3175	P
HD9920116	0	6.9	0.4572	NP	HD9920271	45	4.50	0.2032	P
HD9820223	0	2.5	0.254	P	HD0020087	45	5.45	0.254	P
HD9920028	0	2.6	0.3175	P	HD0020078	45	5.60	0.2286	P
HD9820222	0	3	0.3175	P	HD0020052	45	5.70	0.2032	P
HD9820221	0	4.4	0.2032	P	HD0020077	45	5.93	0.2032	P
HD9920030	0	4.5	0.2286	P	HD9920270	45	6.50	0.2286	P
HD9920115	0	5.7	0.254	P	HD0020113	45	6.59	0.254	P
HD9820220	0	6.6	0.1803	P	HD0020088	45	6.68	0.254	P
HD9920104	0	2.7	0.4064	SP	HD0020153	45	6.81	0.254	P
HD9920040	0	3.1	0.4064	SP	HD0020242	60	2.27	0.1803	NP
HD9920003	0	5.8	0.254	SP	HD0020116	60	2.37	0.2286	NP
HD9920152	0	5.9	0.3175	SP	HD0020171	60	2.63	0.2032	NP
HD9920058	0	5.9	0.2286	SP	HD0020219	60	2.67	0.1600	NP
HD9920014	0	6	0.2032	SP	HD0120003	60	2.76	0.1803	NP
HD9920065	0	6.4	0.254	SP	HD0020170	60	2.93	0.2032	NP
HD9920004	0	6.4	0.2032	SP	HD0120079	60	3.03	0.1803	NP
HD9920032	0	6.4	0.2286	SP	HD0020015	60	3.10	0.2286	NP
HD9920114	0	6.5	0.3175	SP	HD9920275	60	3.10	0.254	NP
HD9820217	0	6.5	0.1803	SP	HD9920274	60	4.30	0.2286	NP
HD9920066	0	6.7	0.4064	SP	HD0020062	60	4.37	0.1803	NP
HD9920009	0	6.7	0.1803	SP	HD0020014	60	4.50	0.2032	NP
HD9920005	0	6.9	0.254	SP	HD0020195	60	4.56	0.2286	NP
HD9920034	0	6.9	0.3175	SP	HD0020169	60	5.09	0.2286	NP
HD0020217	45	2.29	0.2286	NP	HD0020090	60	5.71	0.254	NP
HD0020241	45	2.32	0.2286	NP	HD0020123	60	6.00	0.254	NP
HD0020154	45	2.42	0.4064	NP	HD9920273	60	6.50	0.2032	NP
HD0120055	45	2.48	0.2032	NP	HD0020061	60	6.95	0.2286	NP
HD0020112	45	2.56	0.3175	NP	HD0120004	60	2.66	0.127	P
HD0020194	45	2.63	0.254	NP	HD0020119	60	4.51	0.1600	P
HD0120005	45	2.75	0.2032	NP	HD0020060	60	5.67	0.1803	P
HD0020048	45	3.00	0.4064	NP	HD0020019	60	6.00	0.2032	P
HD0020050	45	4.60	0.4064	NP	HD0020013	60	6.60	0.1803	P
HD0020152	45	5.61	0.4064	NP	HD0020117	60	5.70	0.2032	SP
HD0020121	45	5.69	0.3175	NP	HD0020059	60	5.94	0.2286	NP
HD0020051	45	6.00	0.2286	NP	HD0020118	60	6.80	0.2032	SP
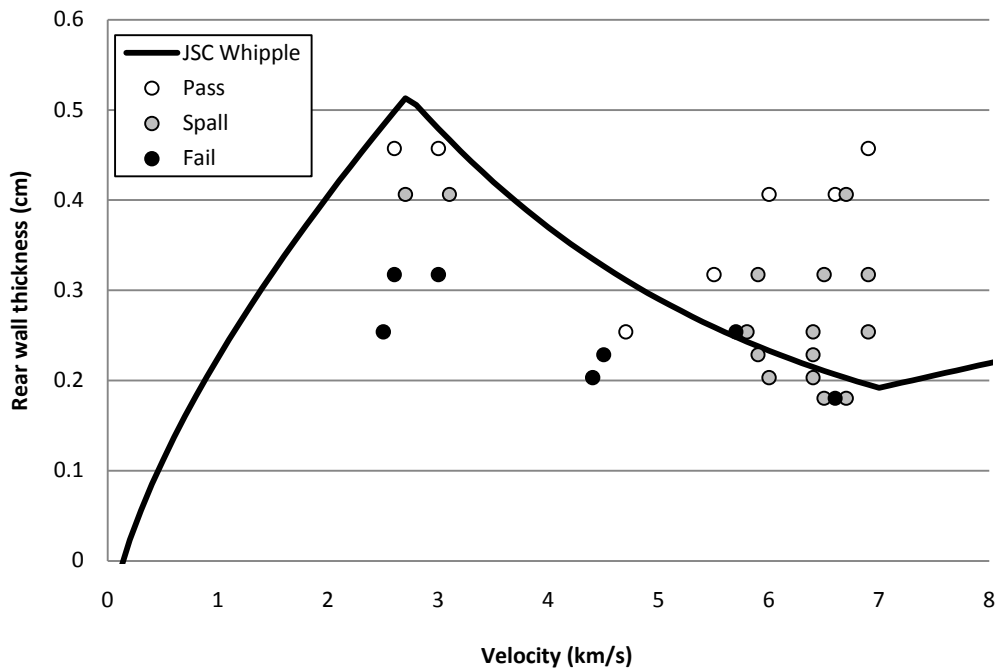
Fig. 5. Results and ballistic limit curves for the normal incidence (0°) tests.
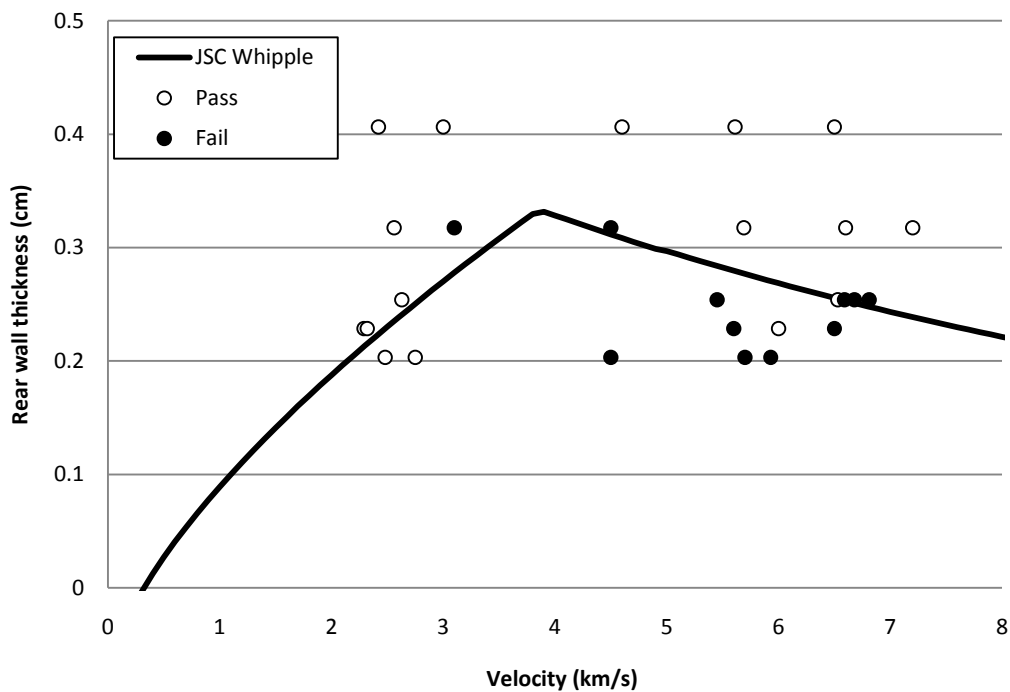

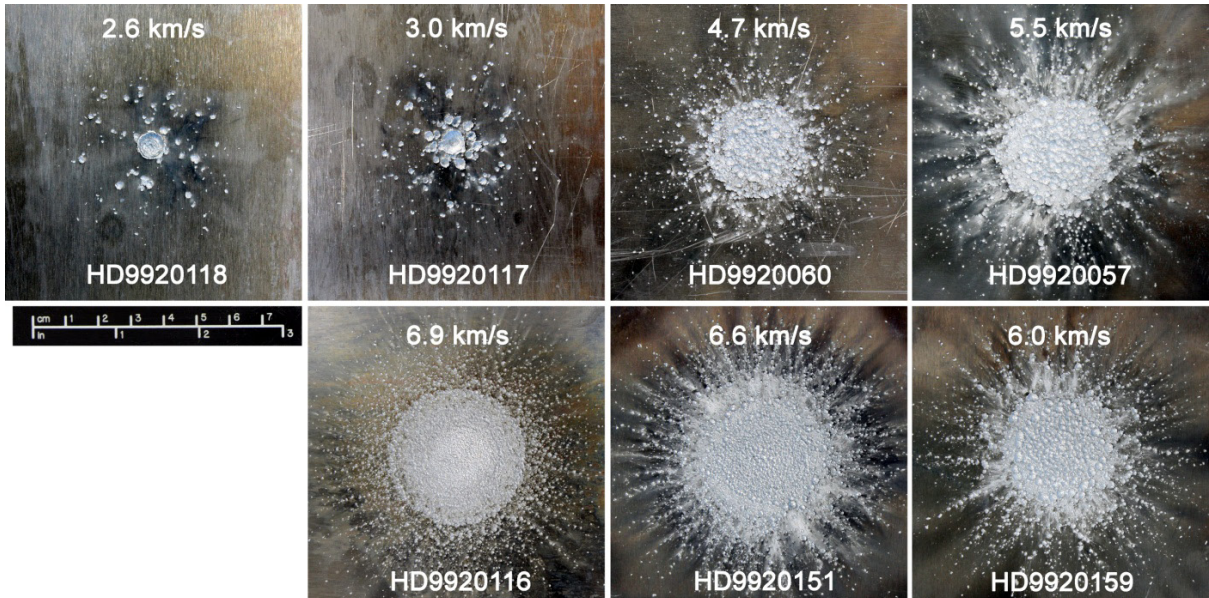Fig. 6. Results and ballistic limit curves for the normal incidence (45°) tests.

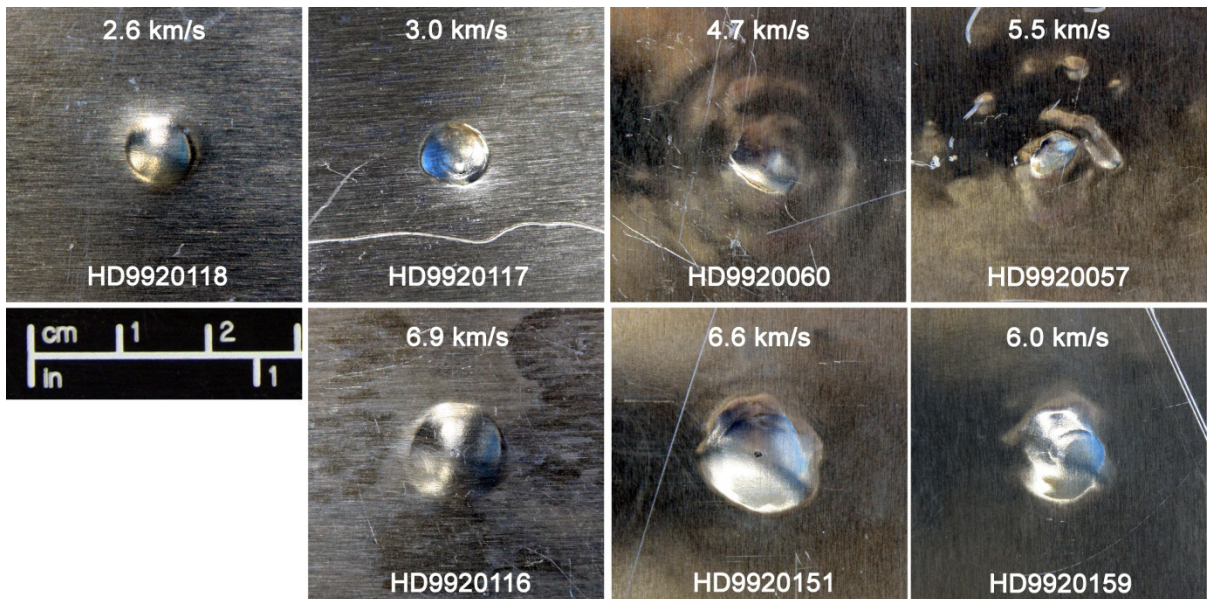Fig. 7. Rear wall (front view) damage profile with increasing impact velocity (clockwise from top left)

Fig. 8. Rear wall (rear view) damage profile with increasing impact velocity (clockwise from top left)

An interesting feature in Fig. 8 is that the lower speed (2.6/3.0 km/s) and higher-speed (6.0/6.6 km/s) tests all show a single, clearly defined bulge (or scab), while the tests at 4.7 and 5.5 km/s demonstrate more complex damage features with multiple fracture zones or bulges.

4. Discussion

The ballistic limit of the Whipple shield configuration tested in this study was shown in Fig. 5 and Fig. 6 to contain additional features in the shatter regime that are not captured in the linear interpolation of current BLEs. These features, however, appear to be well reproduced by the phenomenological curve proposed by Hopkins et al. in [4]. The primary deviation from the linear curve is the increased rate of performance enhancement following incipient fragmentation (i.e. region II), followed by a decrease in performance due to increased kinetic energy of fully fragmented particles prior to the onset of insipient melt (i.e. region III).

Piekutowski [8] investigated the formation of debris clouds during hypervelocity impact, and characterized the largest fragment generated for a variety of bumper thickness to projectile diameter ratios (t_b/d_p) across a range of impact velocities, defined as:

$$d_f = 204.8\,V^{-2.24} \ \ for \ t_b/d_p = 0.049, \ and \tag{8}$$

$$d_f = 147.1\,V^{-2.24} \ \ for \ t_b/d_p = 0.084. \tag{9}$$

where d_f is the largest fragment diameter (mm).

However, an alternate fit can be made to the test data in [8], defined as:

$$d_f/d_p = 5.62e^{-0.86V} \times \left(t_b/d_p\right)^{-0.166V+0.134} \tag{10}$$

A comparison between Eq. (10) and the original relationships derived by Piektowski is made in Fig. 9. For the sake of comparison, Eq.'s (8) and (9) have been extrapolated to larger t_b/d_p values, and are also interpolated for plotting with t_b/d_p as the independent variable. For t_b/d_p ratios in the range characterized by Piekutowski (i.e. 0.049-0.084, see Figure 23 in [8]) the two curves provide similar results, however for t_b/d_p ratios less than 0.049 and greater than 0.084, there is a substantial difference.
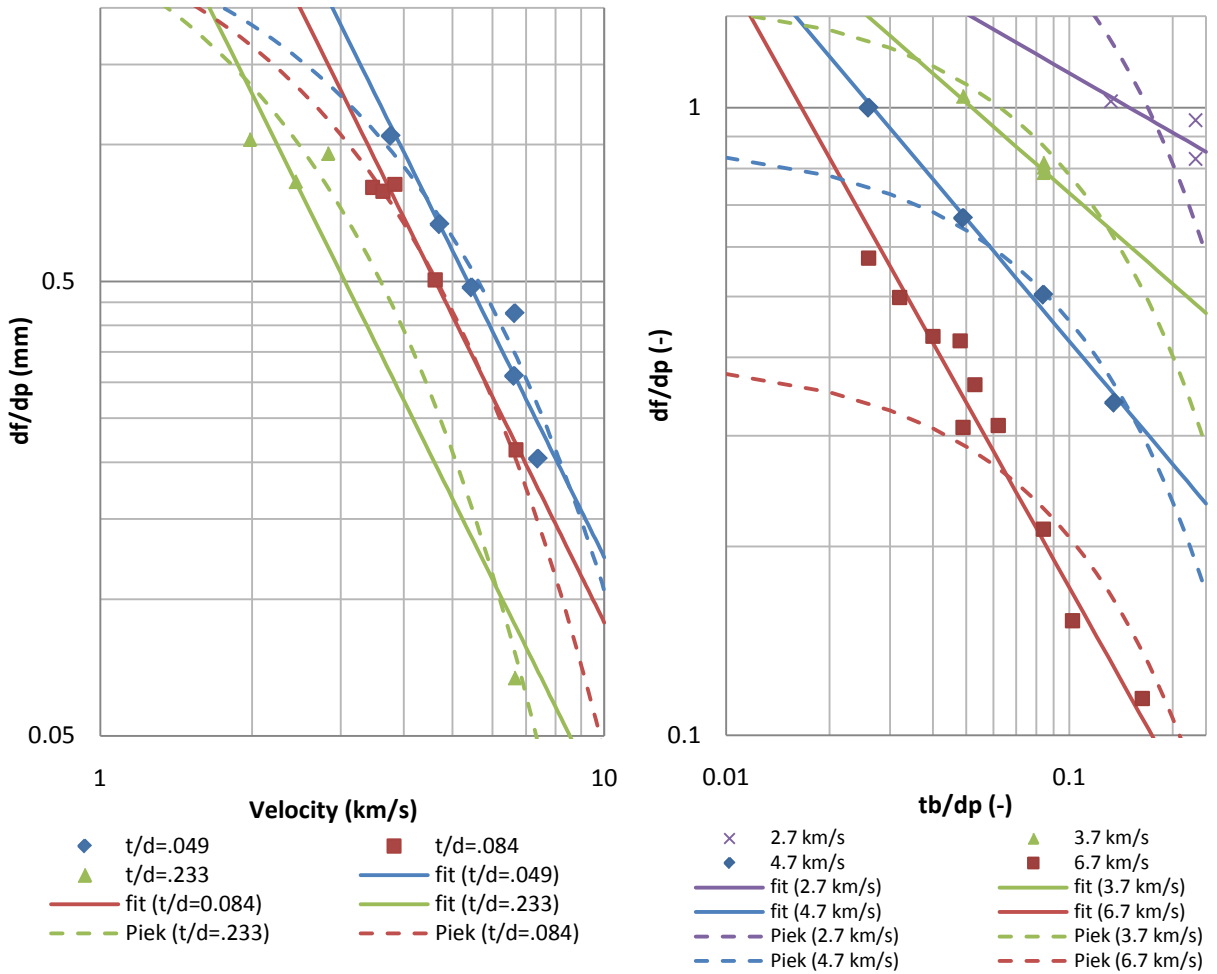
Fig. 9. Comparing largest fragment relationships from Piekutowski (published [8] and extrapolated) and Eq. (10).

If perforation of a Whipple shield rear wall in the initial stages of the shatter regime is assumed to occur due to cratering by the largest fragment in the debris cloud, the ballistic limit can be determined by an extension of Eq. (1). In terms of required rear wall thickness, the ballistic limit is calculated as:

$$t_w = \left(0.6 \, d_f^{\,19/18} \left(\cos\theta \right)^{5/3} \rho_p^{\,1/2} \, V^{2/3} - t_b \right) \left(40/\sigma \right)^{1/2} \qquad (11)$$

Eq. (11) is plotted in Fig. 10 with test data from Table 1 as well as that reported in [4]. It should be noted that the failure criteria used by Hopkins et al. was clear perforation, and as such detached spallation results are not differentiated from pass results. The JSC Whipple shield equation and phenomenological curve from [8] are also included in the figure for comparison.
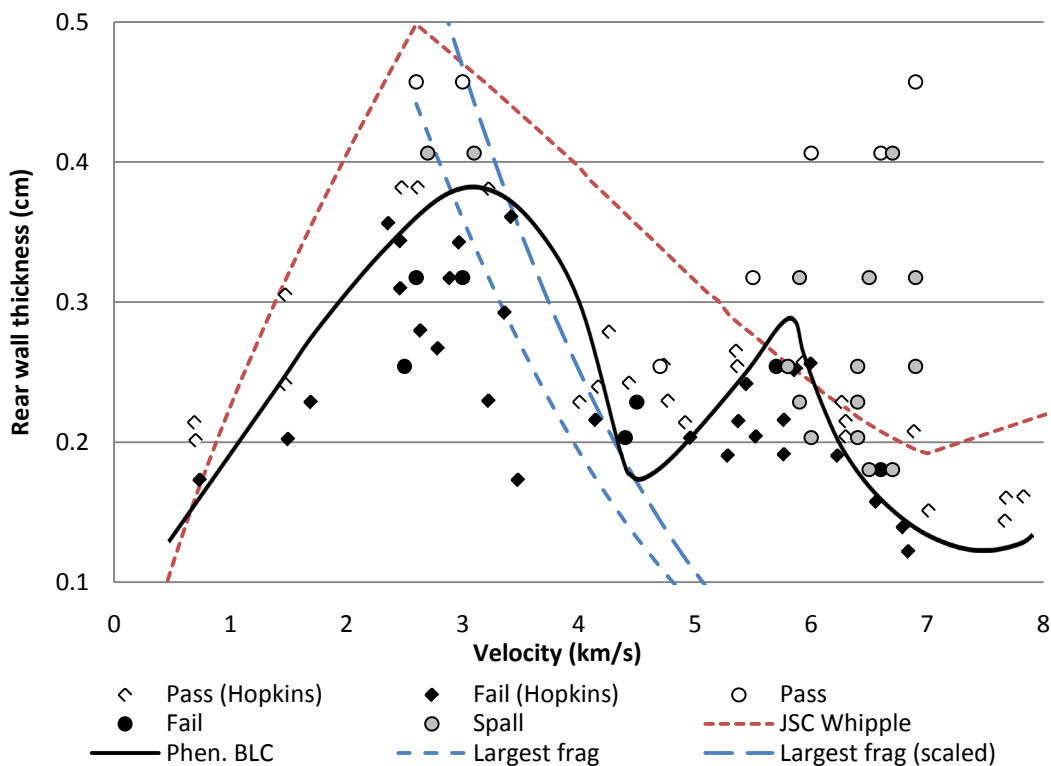

Fig. 10. Largest fragment-based ballistic limit approximation in the shatter regime.

Although the largest fragment approach is shown to be non-conservative for two test results between 3.4-4.1 km/s, the slope of the curve agrees well with the performance decreased noted in this velocity range. A scaling factor of 1.3, when added to Eq. (10), shows an excellent level of agreement with the test results.

A leveling off of required rear wall thickness at approximately 4.0 km/s, extending through until

approximately 5.0 km/s, is observable in Fig. 10. At velocities above 5 km/s, there is a near linear

increase in the rear wall thickness to prevent detached spallation – extending up to 0.41 cm at 6.7 km/s.

To prevent perforation, the required rear wall thickness increases through until 6.0 km/s, followed by a

rapid decrease until approximately 7.0 km/s. Hopkins et al. [4] claim that rear wall damage between 4.4

and 5.6 km/s is due to increased kinetic energy of individual fragments (which remain a constant size).

It is shown in Fig. 9 that the diameter of the largest projectile fragment continues to decrease in this

velocity range, refuting this claim. The assumption of constant fragment size was based on the

appearance of rear wall damage in this velocity range, which remained constant (slight increase in

depth and diameter of individual craters). A radiograph of the internal structure of a debris cloud is

shown in Fig. 11a (from [8]). Although the image is for a lower t_b/d_p ratio (0.046), the characteristics

and key features of the cloud are still relevant, namely: the front element of the cloud is most

effectively shocked (hence the appearance of tiny molten fragments), decreasing in efficiency through

the central element containing the largest fragment, to the rear element or spall shell. The spall shell

contains those fragments of the projectile that are compressed and released by a shock wave that

dissipated a significant percentage of its amplitude, and as such, contains projectile material subject to

the minimum degree of shock heating (demonstrated in Fig. 11b). It is considered that the appearance

of rear wall damage for velocities between 4.0 and 5.6 km/s is dominated by the slow moving, solid

spall shell fragments.

In order to determine the cause of decreasing performance for velocities between ~5.0 and ~6.0

km/s, the rear wall damage features shown in Fig. 8 are of interest. In this velocity range, the

appearance of damage on the rear side of the shield rear wall varies from a single, clearly defined bulge

(or incipient spall), to a chaotic feature with multiple damage sites and no clearly deformed central

zone. It is considered, therefore, that failure in this velocity range is due to the interaction of not only the largest fragment with the rear wall, but is more of a cumulative effect resulting from multiple large fragment impacts. At this time, an analytical description of this behavior (and subsequently an expression for the ballistic limit) is unavailable.
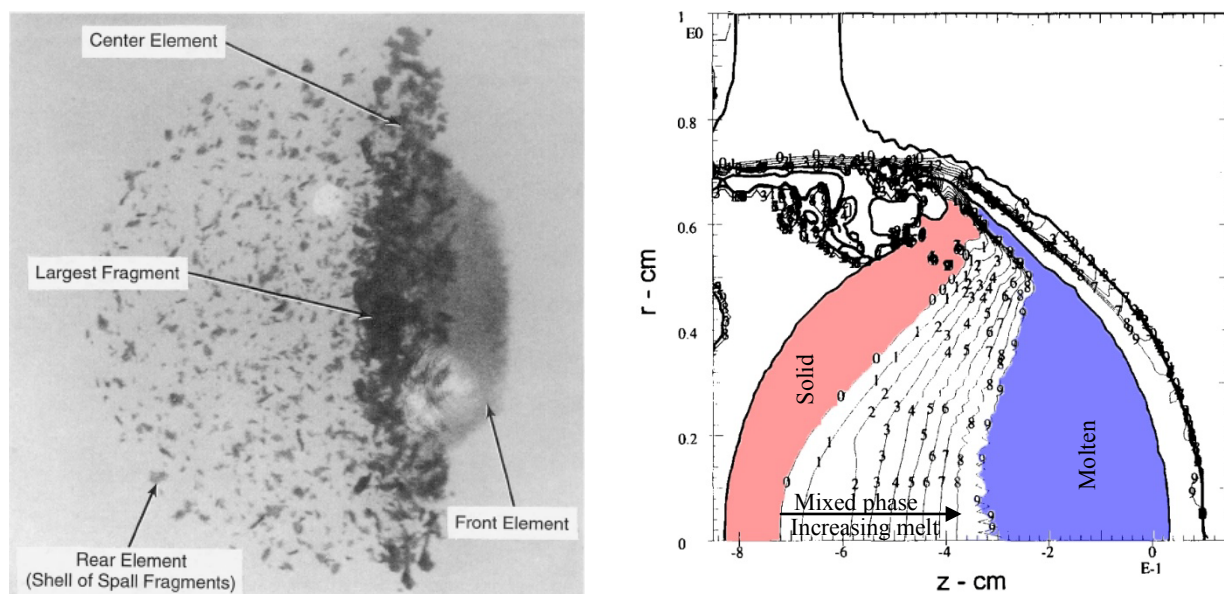

Fig. 11. a) Internal structure of a debris cloud following impact of a 12.7 mm-diameter Al2017-T4 sphere on a 0.59 mm-thick Al6061-T6 bumper plate at 6.26 km/s (from [8]). b) Specific internal energy contours within a projectile during impact at 8 km/s (t_b/d_p=0.2) from solidus (contour 0, 0.67 MJ/kg) to liquidus (contour 9, 1.07 MJ/kg) (from [9]).

Hopkins et al. [4] assume the onset of incipient melt occurs at 5.6 km/s (based on 1D-entropy trapping calculations), which manifests in the BLC as an immediate improvement in shield performance. A more reasonable assumption may be that the effect is only noticeable in the shield performance once a sufficient percentage of the projectile is molten. From the test data, the performance affect appears to begin between 6.0-6.2 km/s. Alme and Rhoades [9] investigated projectile melt for impact on thin aluminum bumper plates using the numerical hydrocode CALE from the Lawrence Livermore National Laboratory. Using enthalpy to determine incipient and complete

melt, simulations of impact at 6.0 km/s showed approximately 20% of the projectile mass had exceeded the incipient melt condition, with 5% at complete melt. Thus, the onset of region IV (defined by Hopkins et al. [4]) should be defined as 6.0 km/s, rather than 5.6 km/s.

5. Summary and Conclusions

The performance of a metallic Whipple shield is described by ballistic limit equations in three parts: low velocity based on cratering relationships, hypervelocity based on momentum conservation, and intermediate velocity (or shatter) as a linear interpolation between the two. Although preferred in terms of computational simplicity, the linear interpolation in the shatter regime may fail to reproduce performance trends previously identified by a number of authors (e.g. [3][4]). In order to investigate the performance of a Whipple shield in the shatter regime, a number of hypervelocity impact tests were performed in which the projectile diameter, bumper thickness, and shield spacing were constant, while the rear wall thickness was varied in order to determine failure limits. Test results were found to agree well with those presented in [4], and demonstrated trends that were not well reproduced by the linear interpolation of the BLE. Following the onset of projectile fragmentation, a much more rapid increase in shield performance was noted between velocities of 3.1 and 4.0 km/s than predicted by the BLE. At velocities between 4.0-5.0 km/s, performance was relatively constant, followed by a decrease between 5.6 and 6.0 km/s for perforation-based failure. For detached spall, the required rear wall thickness was found to increase linearly up to 7 km/s - a result significantly different to that predicted by the BLE.

A re-evaluation of Piekutowski's largest residual fragment size [8] provided the basis for extending the low velocity cratering equation beyond the onset of projectile fragmentation. Although non-conservative, the slope of the derived relationship reproduced the experimental trends well and can be

empirically scaled to match the test data for velocities between 3.0-4.0 km/s. The subsequent decrease in performance is expected to occur as a result of complex interactions between multiple fragment impacts, based on the appearance of rear wall damage (incipient spall feature). To date, there is no analytical procedure to characterize this effect.

The variation of the Whipple shield failure limits in the shatter regime showed a good level of agreement with a phenomenological ballistic limit curve proposed by Hopkins et al. [4]. However, some key features related to complete fragmentation at 4.4 km/s, incipient melt at 5.6 km/s, and complete melt at 7.0 km/s are considered inaccurate. The largest-fragment based analysis showed a continuing decrease in fragment size beyond 4.4 km/s, however this cannot be inferred from inspection of the target rear wall (as done by Hopkins et al.) due to the impact of slower moving solid fragments of the spall shell. Although 5.6 km/s is considered a reasonable estimate for the onset of incipient melt (based on simulation results from Alme and Rhoades [9]), any affect on performance is not expected until a significant percentage of the projectile mass exceeds this condition. From the test results, this appears to occur at approximately 6.0 km/s, relating to 20% incipient melt and 5% complete melt of the projectile mass. The findings of Alme and Rhoades also suggest that the complete melt is not expected to occur until velocities well above 7.0 km/s, as suggested in the phenomenological BLC.

References

[1] Christiansen EL. Design and performance equations for advanced meteoroid and debris shields, *International Journal of Impact Engineering* 1993; **14**: 145-156.

[2] Reimerdes HG, Noelke D, Schaefer FK. Modified Cour-Palais/Christiansen damage equations for double-wall structures, *International Journal of Impact Engineering* 2006; 33: 645-654.

[3] Nysmith CR. A discussion of the modes of failure of bumper-hull structures with application to the

meteoroid hazard, NASA Ames Research Center, Moffett Field, NASA TN D-6039, 1970.

[4] Hopkins AK, Lee TW, Swift HF. Material phase transformation effects upon performance spaced bumper systems, *Journal of Spacecraft* 1972; **9**(5): 342-345.

[5] Schmidt RM, Housen AJ, Piekutowski AJ, Poorman KL. Cadmium simulation of orbital debris shield performance to scaled velocities, *Journal of Spacecraft and Rockets* 1994; **31**(5): 866-877.

[6] Swift H, Preonas D, Dueweke P, Bertke R. Response of materials to impulsive loading, Air Force Materials Laboratory, Wright-Patterson Air Force Base, AFML-TR-70-135, 1970.

[7] Maiden CJ, McMillan A, Sennett R. Thin sheet impact, General Motors Corporation, Santa Barbara, NASA CR-295, 1965.

[8] Piekutowski AJ. Formation and description of debris clouds produced by hypervelocity impact, Univeristy of Dayton Research Institute, Dayton, NASA CR-4707, 1996.

[9] Alme ML, Rhoades CE (Jr). A Computational study of projectile melt in impact with typical Whipple shields, *International Journal of Impact Engineering* 1995; **17**: 1-12.

[10] Cour-Palais B. Meteoroid protection by multiwall structures, *Proc. AIAA Hypervelocity Impact Conference*, Cininnati, USA, 1969, AIAA paper no. 69-372.